ZnO - Nanorod processed PC-SET as the light-harvesting model for plasmontronic fluorescence Sensor

Akhilesh Kumar Gupta[1], Chih-Hsien Hsu[1], Agnes Purwidyantri[2, 4, 9],

Briliant Adhi Prabowo[2, 5, 10], Kuo-Ping Chiu[3], Ching-Hsiang Chen[6],

Ya-Chung Tian[7], Chao-Sung Lai[1, 2, 7, 8,*]

*Corresponding author: cslai@mail.cgu.edu.tw

[1]Department of Electronic Engineering, Chang Gung University, Taoyuan, Taiwan

[2]Biosensor Group, Chang Gung University, Taoyuan, Taiwan

[3]Center for Biomedical Engineering, Chang Gung University, Taoyuan, Taiwan

[4]Research Unit for Clean Technology, Indonesian Institute of Sciences, Bandung, Indonesia

[5]Research Center for Electronics and Telecommunications, Indonesian Institute of Sciences, Bandung, Indonesia

[6]Sustainable Energy Development Center, National Taiwan University of Science & Tech., Taipei, Taiwan

[7]Department of Nephrology, Chang Gung Memorial Hospital, Taoyuan, Taiwan

[8]Department of Materials Engineering, Ming-Chi University of Technology, New Taipei City, Taiwan

[9]Department of Life Sciences, International Iberian Nanotechnology Laboratory, Braga, Portugal

[10]Department of Nanoelectronics Engineering, International Iberian Nanotechnology Laboratory, Braga, Portugal

*Corresponding author:
Prof. Chao-Sung Lai
College of Engineering, Chang Gung University
259 Wen-Hwa 1st Rd, Guishan, Taoyuan 33302, Taiwan
Email: cslai@mail.cgu.edu.tw
Tel: +886-3-2118800 ext. 5607
Fax: + 886-3-2118700

Abstract

This paper reports the combined plasmon coupled - surface energy transfer (PC-SET) and a distance-dependent model constructed by gold nanoparticles (GNPs) over zinc oxide nanorod (ZnO-NR) as a robust and tunable plasmontronic fluorescence regime for the detection of rhodamine 6G (R6G). Further, the deposition of metal created extraordinary contact through ZnO-NR utilizing a rapid thermal process (RTP) allowing the interaction of plasmon-coupled nature and surface energy transfer from the donor (R6G) to the acceptor (ZnO). The percentage of energy transfer efficiency continuously decreased with the increment of GNPs size, shown by 72.93, 67.52 and 47.86%, corresponding to the increase of the distance between the donor and acceptor of 63.03, 67.25, and 82.49 Å, respectively. In other words, the efficiency of PC-SET complied the $1/d^4$ distance dependence model between donor and acceptor molecules with the detection of long-distance ranges from 46.95 – 120 Å. These findings suggest that PC-SET process has a more realistic agreement with experimental outcomes and highly supports quenching efficiency impacts related to the size of GNPs, in which the smaller size of NPs causes' greater effectiveness towards challenges in light harvest enhanced sensing system.

Keywords: ZnO-Nanorods, PC-SET model, light-harvesting, GNPs size effect, Schottky barrier height (SBH), Plasmontronic- fluorescence sensor

1. Introduction

Over the decades, various methods of synthesis and properties of metal oxide composites for the development of sensor applications have been reviewed [1,2]. Among them, noble metal-semiconductor based plasmonic model has gained considerable attention and its coupled nature is a path toward the generation of multidisciplinary research field. In other words, typically coupled nature relies on the interaction between electromagnetic fields and conduction electrons of metal together with semiconductor materials. In general, plasmons are regarded as collective oscillations of the conduction free electrons taking part in the plasmonic model as well as in Maxwell equations. During the past years, many researchers reported advance techniques and methods for plasmonic properties related with surface plasmon polaritons (SPPs) and localized surface plasmons (LSPs) which offer broad applications in spectroscopy,photonics, energy devices and fluorescence sensing devices [3–7]. All these studies comprise a variety of procedures such as absorption, extinction, Rayleigh and Raman scattering, and electron transfer process. Among these phenomena, one of the promising techniques is light-harvesting resonance energy transfer between molecules in the presence of plasmonic materials where the influence of their tunable nature has also been substantially noted [8–10]. On the other hand, noble metal NPs and semiconductor nanomaterial have potential applications due to their excellent plasmonic and photocatalyst properties. In general, the application of zinc oxide (ZnO) as an optical semiconductor material is excellent pertaining to its wide direct bandgap (3.7ev), large exciton binding energy (60 meV) and outstanding thermal stability towards trend for plasmonic applications. Moreover, ZnO is intrinsically defective upon synthesis; these defects are usually with high foundation energies and need to be engineered to make it less defective surface and to contribute charge separation process upon light absorption. Oxygen vacancies and zinc interstitials are two predominant intrinsic

defects mostly reported to be favorable for photocatalysis prospects. Later, Bora et al. reported that ZnO defects could be controlled by annealing at different temperatures for application in optoelectronic devices [11]. The defects have been noted to induce electrons/holes trapping with surface adsorbed oxygen and hydroxyl leading to the formation of O_2^- over ZnO-NR surface. In contrast, metal GNPs and semiconductor material, such as ZnO-NR show essential characteristics such as surface plasmon resonance (SPR) as well as Schottky junction based model. Besides, the understanding of the FÖrster resonance energy transfer (FRET) method between two different dyes or different dipole communication is one of the rising topics nowadays. c A dye is commonly used in the biological system for FRET energy transfer study involving the dipole-dipole interactions between an excited donor (D) and an acceptor (A) molecules. Since the efficiency of FRET depends on the distance of separation between donor and acceptor molecules, the strategy towards GNPs size tunability should be meticulously designed. According to FÖrster theory, FRET technique is restricted up to the upper limit of separation of only 100 Å. According to Persson et al., the validated SET model and mechanism of dye quenching at a metal surface and the separation of donor and acceptor follow the d^4 distance model [12]. In addition, the technique integrating surface energy transfer (SET) between the dye molecule and metal nanoparticles is noteworthy since it enables distance measurement closely twice as far as FRET. Hence, a profound understanding of the large scale surface for photonic applications in the form of light-harvesting models is pivotal. Although these fundamental inventions gained tremendous attention, comparatively little has been discussed or reported concerning the potency of LSPR-coupled FRET for fluorescence enhancement. However, modification of the Jablonski model by combination with plasmonic metal nanostructures and a superior amount of incident energy can be collected by the donors and then transported to the acceptors with improved FRET efficiency.

The enhancement in the emission can be due to resonance energy transfer generally resulted by the distance between the metal-semiconductor and the fluorophore. In this regard, FRET and LSPR could be coupled together to generate a prompt and strong light harvest fluorescence enhancement signal. Some research groups, such as Akhavan et al., reported donor-MNPs-Au acceptor (tri-layer) in which LSP is supported by MNP-mediated energy transfer [13]. Furthermore, Cushing et al. elucidated the control of hot electron injection and the PIRET processes in metal-semiconductor heterojunctions for enhancing photo conversion in a semiconductor [14]. Whereas, Kim et al. reported FRET channels between LSPR-coupled donors and acceptors and discussed in detail about dual enhancement mechanism [15]. On the contrary, the size and shape-dependent surface plasmon resonance (SPR) of metal nanoparticles, such as gold or silver, has been broadly used in FRET-based sensing model in which the catalytic activity of metal NPs is alterable with the size of NPs. The metallic nanoparticles, such as gold nanoparticles, are highly noticed for their excellent characteristics regarding optical ability, high biocompatibility, and high surface area [16]. Additionally, researchers stated that the quenching efficiency of AuNPs increases with the larger particle size due to a substantial enhancement in the extinction coefficient and the spectral overlap between the plasmon absorption band of AuNPs and the fluorescence spectra [17,18]. Some studies denoted that smaller-sized gold nanoparticles reveal stronger fluorescence quenching effects on the molecules near the surface and quenching effects decreases with larger AuNPs size [19–23].

Herein, we introduce a simple, low cost and highly sensitive distance-dependent light-harvesting FRET-based system, involving a novel surface engineered GNPs over ZnO-NR using R6G as donor and ZnO as acceptor. We found out that quantum yield (energy transfer efficiency) changed with different GNPs sizes over ZnO-NR as a consequence of surface area via low-cost

solution-based hydrothermal route followed by annealing at different seeding temperatures in the first process and the optimization toward the development of defectless ZnO surface in the subsequent process. In order to emphasize the plasmonic activity over ZnO-NR, the surface was treated with the gold thin film via thermal evaporation to avoid chemical effects over the device during measurement. The improvement of the engineered gold surface was proven effective by rapid thermal treatment based on the evaluation of GNPs size via RTP with ~60 s duration and interaction of R6G molecule to target the highly analytical optical device as dual enhanced and distance-dependent model. In this manuscript, we present a new perspective of analytical model for light-harvesting based on plasmon interaction with the bandgap energy of the nanostructure semiconductor materials. Moreover, the size and shape of GNPs, and the kind of support will be important factors determining the light-harvesting efficiency of Au-based plasmonic photocatalysts. Overall, the development of light-harvesting PC-SET dual enhanced model could be developed as a potential platform for interdisciplinary work employing optical devices such as in clinical diagnostics, food quality control and drug delivery for biological and chemical applications.

2. Materials and experimental methods

2.1 The synthesis procedure of ZnO-NR on ITO glass

A unique combined structure consisting of GNPs over ZnO-NR based on a low-cost solution process was prepared for this study. The step by step process flow in Figure 1 shows the seeding techniques at different temperatures and growth of ZnO-NR using hydrothermal method for the application in the plasmontronic-energy transfer-based dual enhanced model. In this case, ZnO seed layers were deposited onto ITO coated glass substrate by spin-coating of ZnO precursor solution. The solution was prepared by dissolving 5 mM zinc acetate Zn $(CH_3COO)_2 \cdot 2H_2O$ (99%,

Aldrich) in ethanol (Aldrich). Finally, the as-deposited film substrates were annealed at 400, 450 and 500°C in air for 30 minutes, respectively, to create ZnO seed layer on ITO. Next, the sustained seed layer was dipped vertically into an autoclave Teflon container with an aqueous solution of equimolar zinc acetate and hexamethylenetetramine ($C_6H_{12}N_4$) (Aldrich) for nanorod growth (1x1 cm^2) in 8 hours.

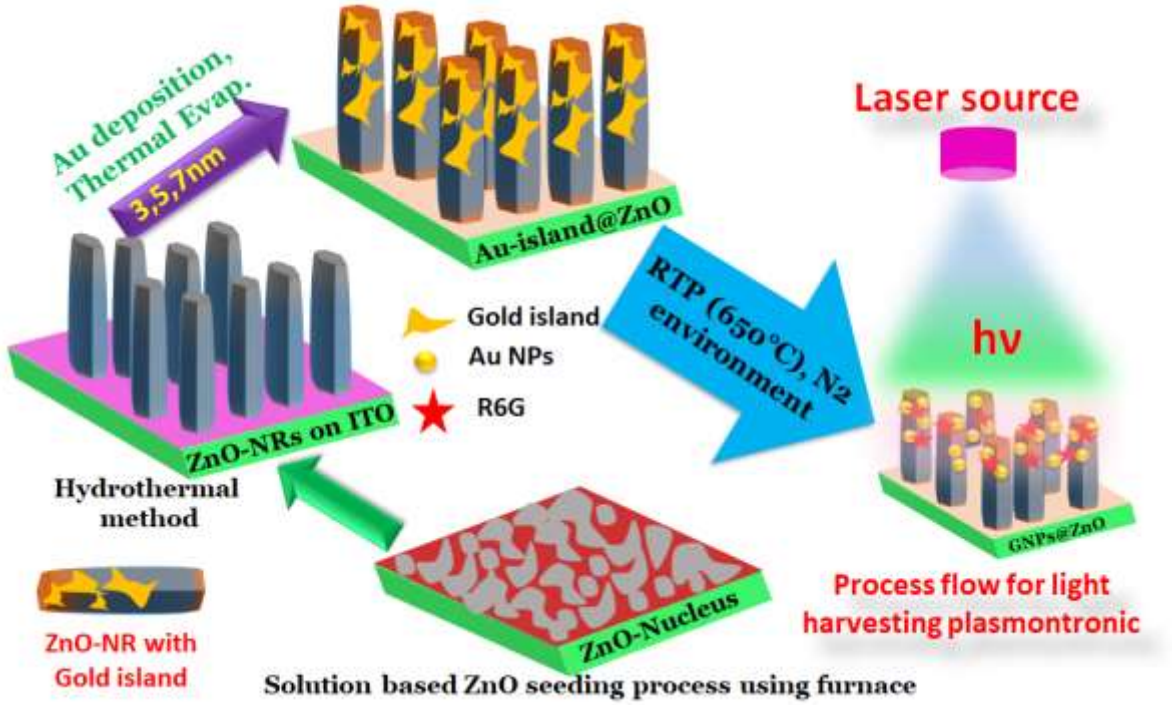

Fig. 1. Schematic diagram of the experimental process as light-harvesting plasmontronic model

2.2 ZnO-NRs based plasmontronic – SET electrodes

After the growing process of ZnO-NR, different gold layer thickness over ZnO-NR via thermal evaporator was deposited at 3, 5 and 7 nm, respectively. For the deposition of gold, evaporation method was conducted to avoid chemical methods and reactions over the sensing area. In addition to the creation of GNPs over ZnO-NR, rapid thermal process (RTP) at 650°C with 60 seconds over the gold-coated surface was employed to generate the GNP islands. X-ray diffraction (XRD) analysis of ZnO Nanorods and composite with GNPs were examined using a Cu Kα radiation (Bruker Germany). Surface morphological images and elemental analysis were taken from field

emission scanning electron microscope combined with energy-dispersive spectroscopy (EDS) (FE-SEM, JEOL JSM-7500F). Thermal evaporator with a deposition rate of 1 Å/s under 10^6 m Torr pressure adjustment was applied. Rapid Thermal Anneal model SJ-RTA1000M-V (SJ High Technology, Taiwan) was used afterward to generate Au nano-island structure. Time-resolved measurements (TRPL) were made with 405 nm excitation and analyzed using time measurement histogram accumulating real-time processor by UniDRON with TCSPC (UniNano Biotech Co., Ltd., New Taipei, Taiwan). The fluorescence lifetime was fitted by a bi-exponential decay model using Fluo-Fit software.

2.3 Fluorescence signal detection based on nanomaterial

Fluorescence detection is a powerful tool with a comprehensive range of applications in chemical and biological sciences. The need for ultrasensitive biological and chemical assay and the trend towards the biofunctionalization of nanomaterial has developed one of the newest fields in optical devices [24]. Due to the unique properties of nanomaterial, the biofunctionalized nanoparticles can yield a synergistic outcome in catalytic activity and biocompatibility to signal amplification in a new generation nanosensing optical devices. Mostly, metal nanoparticles promote direct electron transfer between the biomolecules and electrode surface and have a great ability for specific recognition and signal detection in optical, electrochemical, and photo-electrochemical models [25]. Among them, plasmontronic is one of the emerging techniques that takes advantage of plasmon electron properties to yield novel interactions between metal-semiconductor devices. To validate plasmontronic effect due to metal-semiconductor, we put R6G (10^{-4}M) at the device and dried it over the surface to measure its response using the TRPL measurement method for possible conditions.

3. Results and discussion

3.1 Surface Characterization and proposed device model

The synthesized ZnO Nanorods and gold decorated ZnO sample was examined by XRD, FE-SEM, and EDX analysis for structural and morphological identification. Fig. 2 (A) describes the nature of the hexagonal ZnO-NR with corresponding peaks of (100), (002), (101), (102) planes. After the decoration of gold over ZnO surface, newly (111) peaks were generated as a consequence of the deposition of gold (Inset) Fig. 2(B). All the peaks of ZnO could be indexed to hexagonal ZnO with lattice constants of a = 3.285, c = 5.126. The spacing values and relative intensities of the peaks greatly coincide with the JCPDS card no. 36-1451 for ZnO and 65-2879 for Au [26]. The effects of ZnO seeding temperature on the morphological properties of the structure were shown in the change of ZnO-NRs diameter and density at 400, 450 and 500 °C seeding temperatures, respectively, where the length of NRs was approximately 1.5 to 2 µm as displayed in Fig. 2B by cross section of ZnO-NR [27]. It is denoted that the diameters of the nanorods were also increased with the higher pre-annealing temperature of the seed layers, which may be due to the enhancement of the grain size of the seed layers. However, the formed nanostructures significantly affected the photon absorption efficiency at different annealing temperatures due to different morphology of ZnO-NRs. Similar results were reported previously by other groups in which clearly relate to solution method and seeding temperature [28]. RTP plays an important role on the island surface properties and is considered as one of GNPs patterning techniques over ZnO-NR in correlation with gold layer thickness [29].

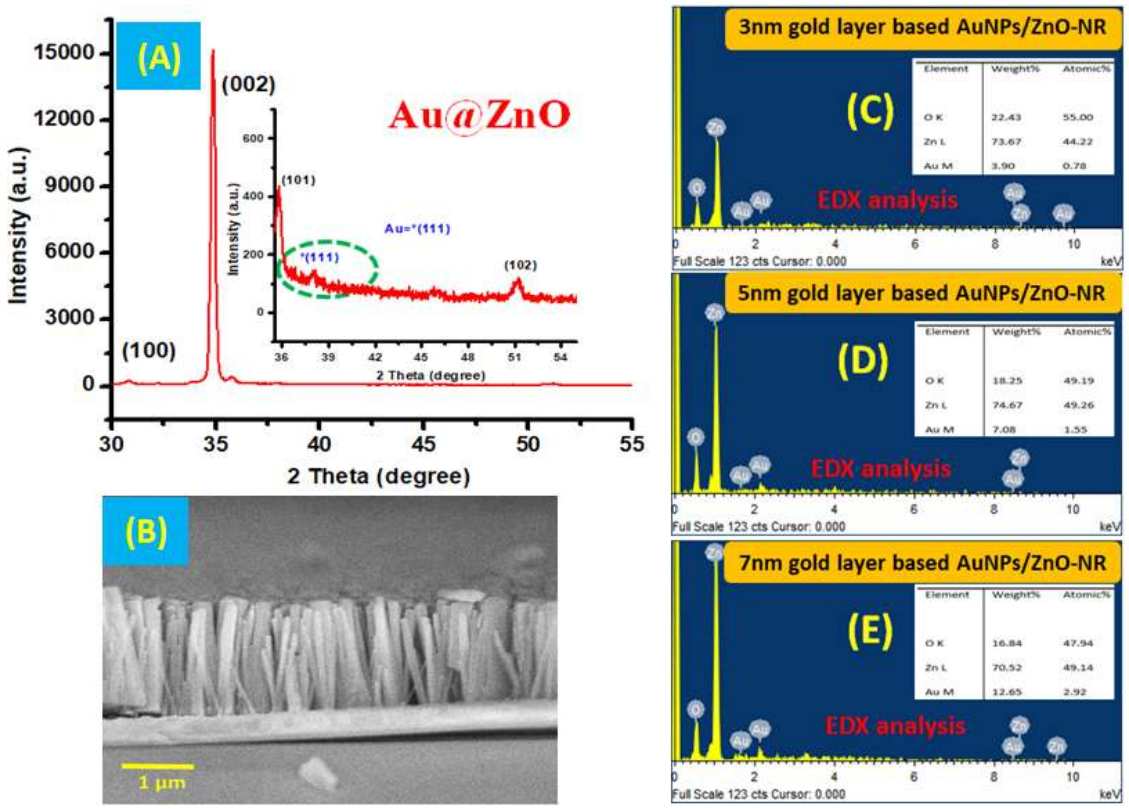

Fig.2 (A) XRD analysis of ZnO-NR & Au over ZnO-NR (Inset Fig.) (B) The length of ZnO-NR (C-E) EDX analysis of GNPs over ZnO-NR and its atomic % effect due to gold thickness layer

In Fig. 2 (C, D, and E), the EDX measurement confirmed the presence of gold atomic content over the ZnO-NR surface. The atomic content of Au showed the tendency to elevate after the decoration of ZnO-NR with Au film, with the percentage of 0.78 %, 1.55 %, and 2.92 % for deposited Au film with the thickness of 3, 5 and 7 nm, respectively. In contrast, from Raman spectrum analysis, we observed that ZnO-NR grown under different seeding temperatures demonstrated peak reduction with the higher seeding temperature. This indicates the oxygen vacancy can be suppressed successfully as well as the improvement of the crystalline structure with decreasing oxygen vacancy [27].

A similar concept from photoluminescence measurement and the defects modeled during the chemical process were likely to be an oxygen vacancy and interstitial oxygen pertaining to the green and yellow bands in PL. From the defect point of view, there are two types of oxygen defects

which belong to green and yellow bands. Two impurity levels boosting the electron-hole pair separation rate in ZnO Nanorods are produced in the presence of oxygen vacancies and interstitial oxygen defects. The drop of PL emission intensity as the effect of higher annealing temperature implies the reduction of oxygen defects in ZnO-NRs [30]. Outcomes indicate that after the deposition of GNPs over ZnO-NR with different surface defect densities, the establishment of the Schottky junction between Au and ZnO is affected. Similar results were reported by Bora et al. which revealed that at the higher annealing temperature of ZnO-NR, the surface defects were minimized. The phenomenon confirms easy injection of the electrons during the Schottky junction model (SBH) and temperature effects as shown in schematic Fig. 3C [31]. Not only that, the same concept was claimed by Hwang et al., in a study of GNPs@ ZnO-NR interface annealing at 450°C which retained the lowest barrier height (0.67 eV) in comparison to the samples annealed at 350°C with a barrier height of 0.72 eV [32]. From the above discussion, it is notable that oxygen vacancy and surface defects on the ZnO surface also plays a vital role in photocatalytic and surface plasmonic activity [33]. Furthermore, Fig S7 Illustrates the UV–Vis absorption spectra of ZnO and different size of GNPs over ZnO due to RTA treatment over the surface. ZnO-NR shows no band at visible region as well as no plasmon nature. But the spectrum of nanocomposite at different size of GNPs clearly display an absorption in the visible region attributed to the localized surface plasmon band at around 500 to 660 nm wavelength. However, in this research, high density of GNPs was well distributed over ZnO-NR via RTP treatment and found to be actively taking part for a plasmonic PC-SET dual distance-dependent energy transfer for optoelectronic applications.

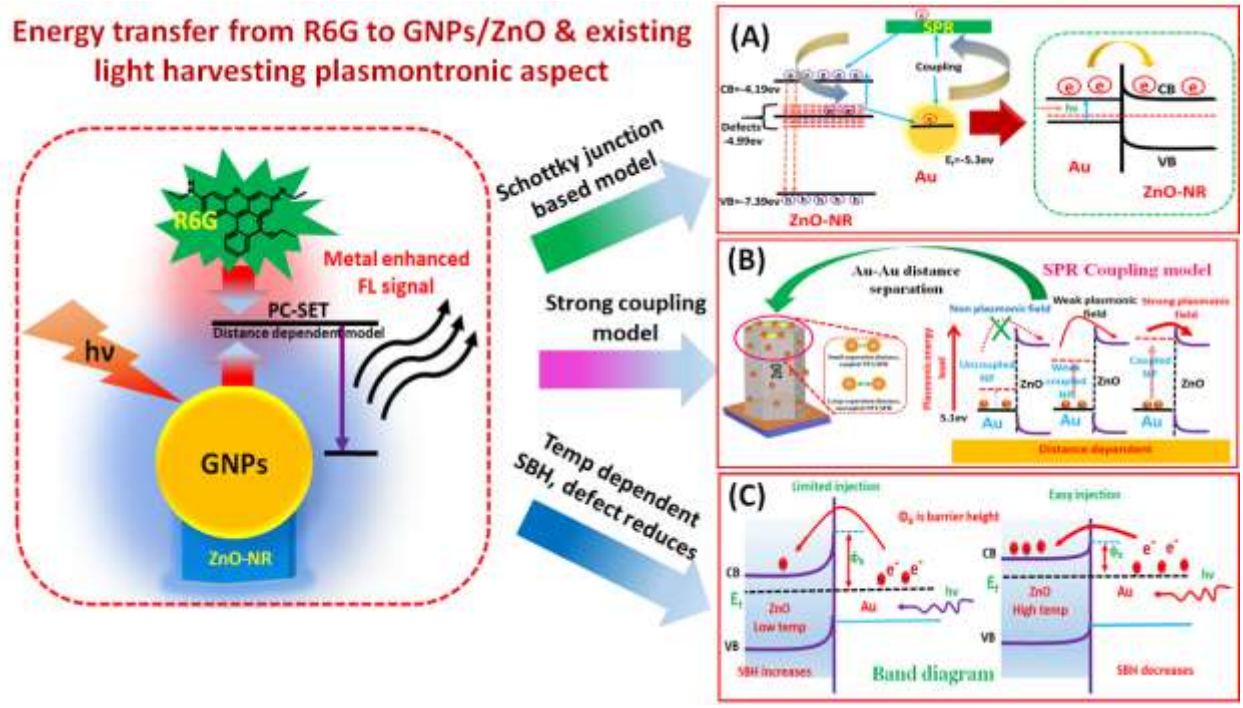

Fig.3 Illustration of mechanism & plasmontronic-fluorescence signal detection model (A) Schottky junction based plasmonic model and energy diagram (B) coupling between gold nanoparticles and distance aspect ratio (C) Energy diagram of temperature-dependent Schottky barrier height (SBH) model

From previously reported data, we summarized the proposed theory of LSPR-FRET and distance-dependent model focusing on the existing models in PC-SET as plasmon coupled aspects for light harvest fluorescence sensing model. Thus, existing models connected with PC-SET are (A) Schottky junction-based plasmonic model and energy diagram explaining the detail mechanism of plasmon excitation of GNPs over ZnO-NR and the suitability of energy diagram for electron injection as well as the transfer of the electrons to fulfill SPR signal existence model [34]. (B) The GNPs which essentially contributes in coupling interaction. These coupling interactions should depend not only on the distance for the coupling between GNPs, but also on energy similarly possessed by these waves coupling between gold nanoparticles themselves in regards with distance and particle aspect ratio or diameter [35,36]. (C) Energy diagram of temperature-dependent Schottky barrier height (SBH) in which was found here that at high-temperature, SBH

would be reduced and electron could be injected easily from metal to semiconductor to form a route for plasmonic appearance [31]. The detailed schematic and explanation of energy diagram as development of light-harvesting plasmontronic fluorescence can be seen in Fig. 3.

3.2 Modified Jablonski diagram and dual enhanced light-harvesting mechanism of energy transfer

As previously studied by many research groups, transfer of energy and distance-dependent theory near metallic islands are mostly employed. However, applying metal-enhanced fluorescence (MEF) and interface with ZnO semiconductor as PC-SET dual enhanced model have emerged as a potential new core technique in optical devices [37]. Therefore, demonstrations and applications of MEF with semiconductor exploiting the effect of local field enhancement generated near metallic structures are considered novel techniques [38]. Metals can intensely interact with the incident light and yield concerted electrical fields with a localized charge density oscillation. In general as per classical Jablonski diagram, photon absorption results in a fluorophore in the first singlet state S1. The fluorophore can then emit a photon or radiate energy with a rate constant Γ, which is called as the radiative decay rate. The fluorophore can also return to the ground state by non-radiative decay with a rate (K_{nr}) or due to some other quenching process (K_q). The quantum yield (Q_0) of a fluorophore reflects a competition between emission of a photon and the non-radiative decay process.

$$Q_0 = \frac{\Gamma}{\Gamma + K_{nr} + K_q} \quad \text{----------(1)}$$

The fluorescence lifetime or decay time is the meantime a fluorophore remains in the S1 state and is given by:

$$\tau_0 = \frac{1}{\Gamma + K_{nr} + K_q} \quad \text{----------(2)}$$

The unique possibilities for modified Jablonski diagram are due to changes in excitation and emission levels. A metal particle can amplify the incident light field by interactions of the light with the free mobile electrons in the metal. For a fluorophore at an appropriate distance from a metal surface, the quantum yield (Qm) and lifetime (τm) are given by:

$$Q_m = \frac{\Gamma + \Gamma_m}{\Gamma + \Gamma_m + K_{nr} + K_q} \quad \text{----------(3)}$$

$$\tau_m = \frac{1}{\Gamma + \Gamma_m + K_{nr} + K_q} \quad \text{----------(4)}$$

Notably, under the same conditions, the proximity of a fluorophore to a metal can increase the radiative rate due to addition of Γm. This increases the quantum yield and decreases the lifetime. The fluorescent molecule (R6G) near the metal surface shows a competent coupling between the electromagnetic field and spatially confined free-electrons indicating higher emission intensity in the form of fluorescence [39]. Another substantial factor in this technique is the plasmon-coupling effect facilitated by a non-radiative interaction. If the plasmon and the fluorophore are at an optimal distance, the energy transfer between them is dominated [40]. However, surface energy transfer (SET) networks between LSPR-coupled donor and acceptor as the dual enhanced mechanism based on FRET theory and LSPR can be coupled to induce strong light harvesting fluorescence signal as presented in Fig. 4 (A).

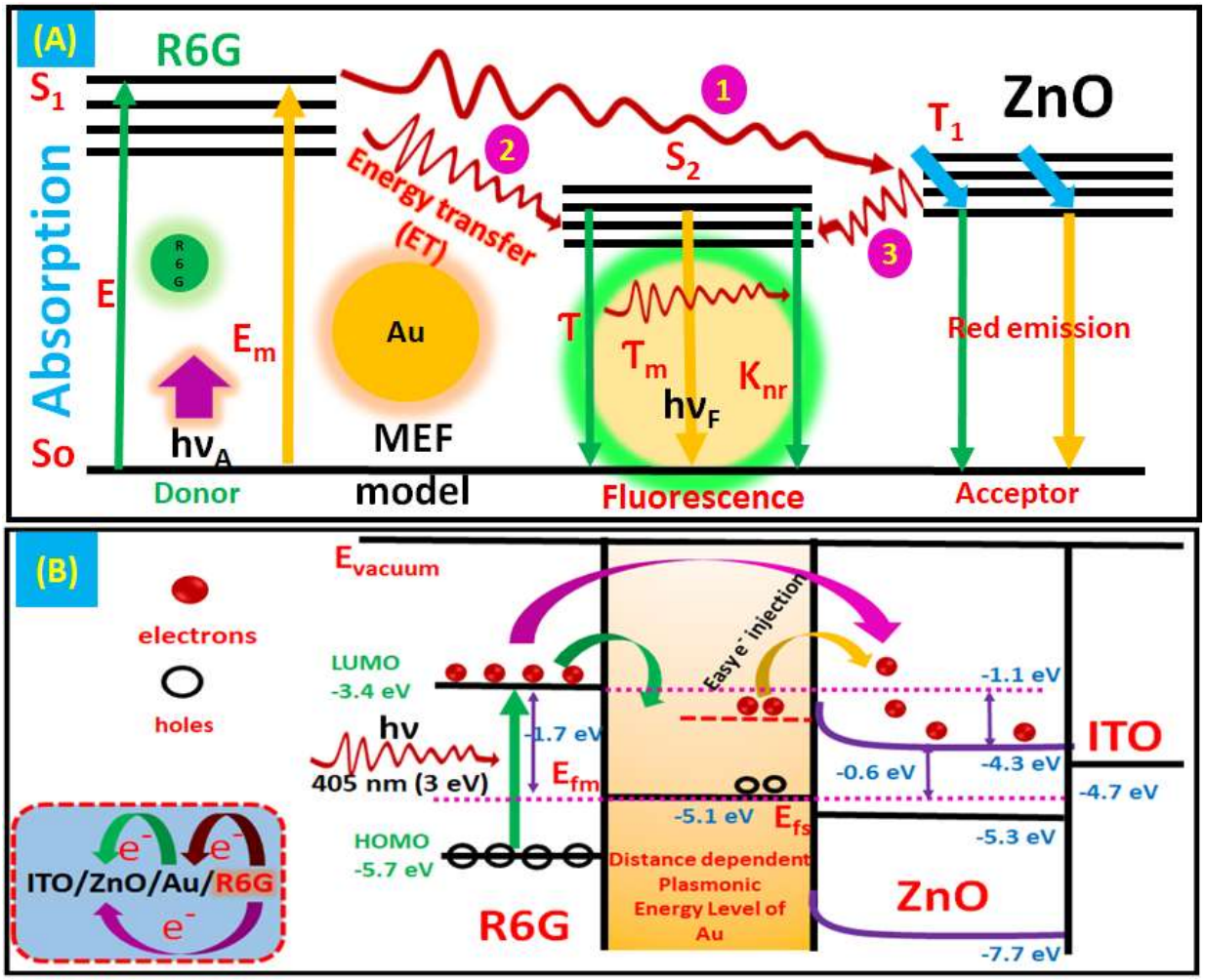

Fig. 4 (A) Modified Jablonski diagram with fluorophore-metal-semiconductor interactions (B) Energy level diagram and possible electron transfer mechanism of Au/ZnO system in the presence of R6G (LSPR & SET as dual enhancement mechanism & model)

Consequently, during lifetime measurement, no noticeable change in thelifetime was observed for the control sample (Table S1), yet, the mechanism might be different from that in metal-enhanced fluorescence (MEF) based PC-SET model. Our objective was to control the lifetime using a different substrate with and without GNP over ZnO-NR as explained in energy transfer model-based TRPL. Conversely, the development of energy transfer model at the Au/ZnO interface can be explained from the energy diagram in which a Schottky barrier generated when the work function of the metal (5.1 eV) is higher than the electron affinity of the semiconductor (4.3 eV). In

the first step upon excitation of light (405 nm), the electrons from the lowest unoccupied molecular orbital (LUMO) of dye are transported to the conduction band of ZnO via tunneling effect across a thin layer of gold. In the second step, upon excitation of light absorbed by the dye, the injected electrons into the gold nanoparticles embedded in the surface of the ZnO-NR trigger the accumulation of electrons in the Au nanoparticles. As a result, the Fermi energy of the Au nanoparticles is dragged closer to the conduction band (CB) of the ZnO and the transfer of electrons from the Au nanoparticles to the CB of ZnO could occur to establish charge equilibrium in the system as presented in Fig. (4B). Additionally, a similar mechanism has been reported where the Schottky barrier formed at the Au–ZnO interface reduces the charge recombination by blocking the transfer of electrons from ZnO to the dye and thus, improving the characteristics of DSSC solar cells [9,41].

3.3 Time-Resolved photoluminescence (TRPL) Study & development of light-harvesting PC-SET dual enhanced model:

The time-resolved photoluminescence (TRPL) aqueous solution of R6G dye in the presence of GNPs over ZnO-NR as plasmonic energy transfer model is depicted in Fig. (5-7). For the TRPL study, a lifetime of R6G, ZnO and related composite hybrid materials at the different conditions with the tunable size of GNPs can be used to investigate the charge transfer deactivation process during reactions. Here, we also reported non-plasmonic and plasmonic energy transfer without GNPs as R6G/ITO, R6G/Au/ITO and R6G/RTP-Au/ITO analyzed from TRPL data in the supplementary material (Table. S1). It was analyzed that the system was less effective without ZnO-NR in control sample as shown in Fig. S1. In this context, the fast decay component (T_1) can be attributed to non-radiative recombination originating from free exciton state, and slow decay component (T_2) is ascribed to radiative bound exciton states [42]. From bi-exponential fitting data,

component (T_1) and (T_2) vary after the decoration of gold over ZnO-NR with composite materials and tunable nature of GNPs size as well as the average lifetime.

TRPL Bi-exponential profile was fitted with this following equation

$$I(t) = A_1 \exp\left(\frac{-t}{\tau_1}\right) + A_2 \exp\left(\frac{-t}{\tau_2}\right) \text{ ----------(5)}$$

Where I (t) is intensity, τ_1 and τ_2 are decay times, and A_1 and A_2 are relative magnitudes.

Average lifetime $\tau_{av} = \left(\sum A_i \tau_i^2 / \sum A_i \tau_i\right)$ ----------(6)

The photoluminescence decay time of the R6G dye solution without gold is a single exponential model, and the value is 3.51 ns in which the decay lifetimes of dye molecules in the presence of GNPs over ZnO-NR are fitted by bi-exponential decay (eq.5). The tabulated data (Table.S2) summarizes the time constants and relative amplitudes for three different seeding temperature of ZnO-NR grown and compares them by bi-exponential fits. According to the reported PL studies, the seeding temperature at 400 and 450°C exhibit an extrinsic defect over ZnO surface with the low performance for a stable device due to surface defects (Table S2 (A-B)) [43]. In our study, at 500°C, high temperature-annealed ZnO had fewer defects and its results were consistent with reported data as well as its intrinsic nature as demonstrated in Fig. 7B. As can be checked (Table S2(C)), at 500°C seeding temperature, the fast components are 3.97, 4.49 and 5.21 ns and slow components are 0.20, 0.18 and 0.21 ns with R6G dye solution in the presence of GNPs over ZnO-NR. The average lifetime increased with the value of 0.95, 1.14, and 1.83 ns, respectively, following the subsequent thickness of 3, 5 and 7 nm GNPs layer over ZnO-NR. This finding confirms the plasmon coupled-SET as a dual enhanced energy transfer model as shown in the drop of an average lifetime from 1.25 to 0.95 ns in the presence of GNPs over ZnO after RTP treatment

whichapparently proves the transfer of energy from donor to acceptor. This outcome is in a good agreement with previously reported work on the fluorescence lifetime decrement when R6G interacting with the spherical, shaped, and capped Au NPs [44].

Hende, the energy transfer efficiency from dye to Au nanoparticles can be calculated by using this equation:

$$ET(\%) = 1 - \left(\tau_{DA} / \tau_{D} \right) \text{ ----------(7)}$$

From previously reported works of literature, a significant number of theoretical modeling and experiments has claimed that the molecular interaction of a dye with a dipole is damped by the reaction of a nearby metal NPs [45,46]. Moreover, quenching and enhancing of the fluorophore intensity are linked to a space mechanism connecting the dipole of the donor and the gold NP as acceptor as the possible interfaces with free electrons. Researchers also reported that because small metal NPs are not actively involved in the SPR mechanism, they cannot accept more energy on the surface [18,47]. Another aspect is that smaller NPs are better for a plasmonic model and its related applications [19,22,48,49]. However, the smaller GNP size is highly noted to be the least intrusive component in biological system and applications. A previous study has reported that the efficiency of FRET depends on the inversed sixth power of the distance of separation between donor and acceptor. However, FRET model is restricted on the upper limit of only 100 Å because the energy transfer becomes too weak [50]. Using similar postulation, Chance et al. described the rate of energy transfer from a dipole to a metallic surface and interband transition [45]. This was further extended by Persson et al., to the metal's conduction electrons and known as surface energy transfer (SET) [12]. Later, Gersten-Nitzan models were also used for the modeling of dipole-dipole interactions with plasmonic gold NPs, however, it's not suitable to explain both the distance dependence and quenching efficiency of dye together precisely [51]. According to Persson and

Lang model, the momentum and energy conservation in the dipole induces the creation of electron-hole pairs on a surface and is also suitable and useful for modeling this system [12]. Because of this model, the rate of energy transfer is calculated using the Fermi golden rule which is related to excited-state molecule with the simultaneous scattering of an electron in the neighboring metal to above the Fermi level. However, in regards with the conservation of momentum, to be considered plasmonic, the excitation of an electron-hole pair must coincide with an electron-electron and electron-surface potential scattering. Based on Persson model, the detail derivation of the damping rate to a surface of a noble metal is presented in the supporting file wherein final, the distance between donor and acceptor was obtained by using the following formula:

$$d = d_0\left(\frac{1}{ET} - 1\right)^{1/4} \quad \text{---------- (8)}$$

From the proposed above model, the calculated d values between donor and acceptors at all possible condition and together with three different seeding temperatures of ZnO-NR can be explained (Table S2). From equation (4), the efficiency of (surface energy transfer) SET depends on the inverse fourth power of the distance and separation between donor and acceptors, d0 represents the quenching distance (details can be found in the supplementary file with help of Eq.4 to 6). From the tabulated d values and TRPL, the distance value changes along with the size of GNPs, respectively. We can see that at 400 & 450°C seeding temperature of ZnO, the distance between donor and acceptor values dropped from 120, 111 to 64.83 & 52.15 Å altogether with the changes of GNPs size as displayed in in Fig.5 & 6 (A, B and C). From the graphs, it is noticeable that the energy transfer efficiency (ET %) and distance dependence are inconsistent with each other. But at 500°C seeding temperature of ZnO, the distance between donor and acceptor leveled up from 63.03 to 82.49 Å altogether with the changes of GNPs size as well as the

loss of ET efficiency (%). From Fig.7 (A, B, C), it is elucidated that energy transfer efficiency (ET) and distance dependence are opposite and consistent with each other. This outcome follows well the plasmon coupled-SET proposed a model for a strong dual enhanced nature of the device. More importantly, it was observed that the attachment of dye molecules also varied with the shape-changing of Au nanoparticles. It is exciting to note that a similar trend is observed in the FRET-based model, but its values are restricted to the upper limit of 100 Å. Hence, in the present study, it is indicative that the energy transfer process from dye to GNPs over ZnO follows a surface energy transfer (SET) process and a $1/d^4$ distance dependence model.

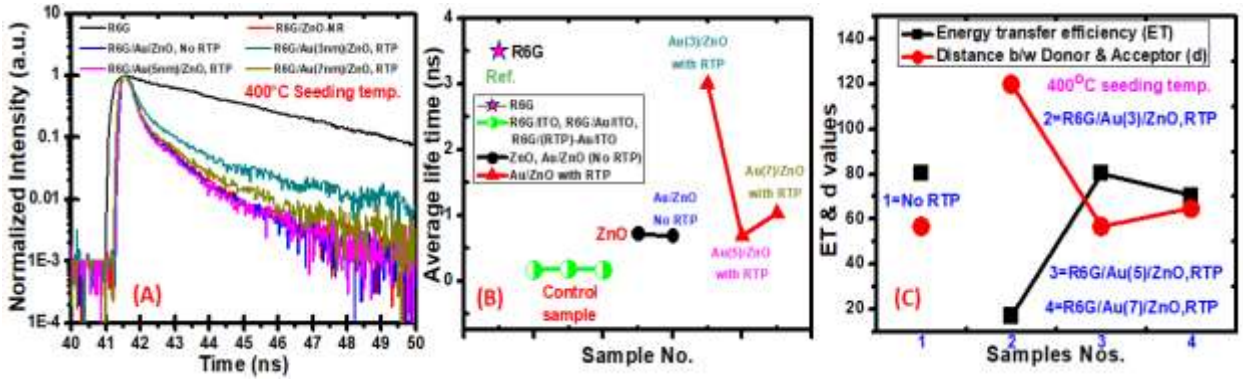

Fig.5 Time Constants (τ) and Relative Amplitudes, and Bi-Exponential Fits of the PL Decay Profiles for (A) TRPL response at 400°C; and (B) Average lifetime and (C) respective energy transfer and distance-dependent values related to GNPs size over ZnO-NR

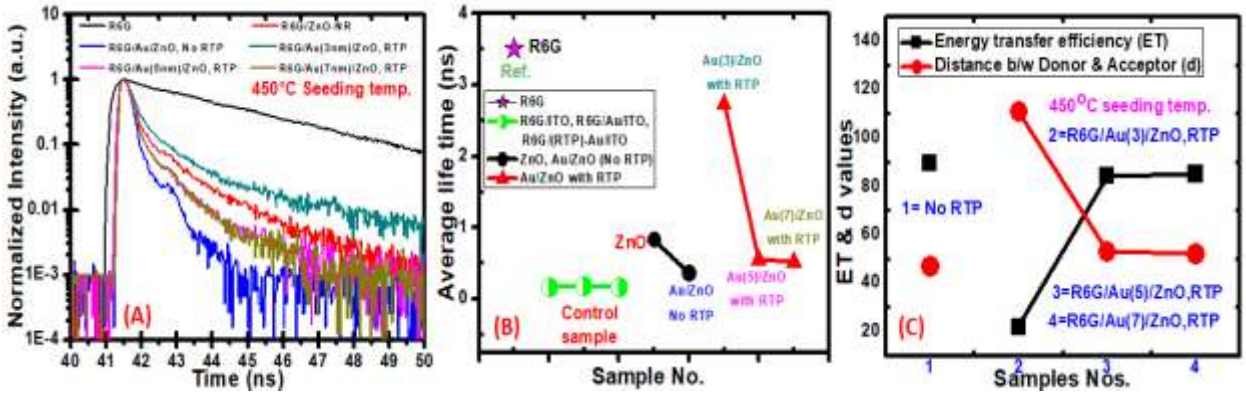

Fig.6 Time Constants (τ) and Relative Amplitudes and Bi-Exponential Fits of the PL Decay Profiles for (A) TRPL response at 450°C; and (B) Average lifetime and(C) respective energy transfer and distance-dependent values `related to GNPs size over ZnO-NR

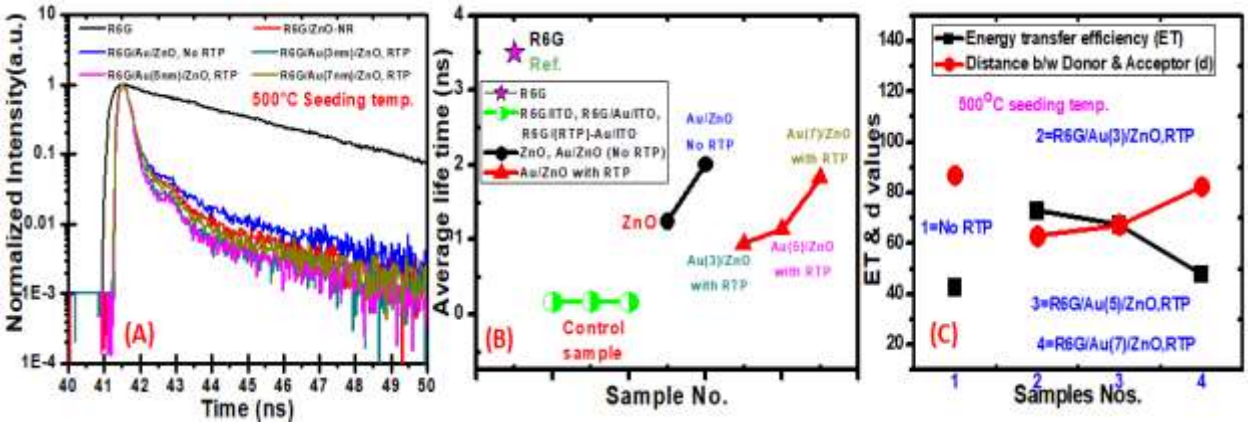

Fig.7 Time Constants (τ) and Relative Amplitudes and Bi-Exponential Fits of the PL Decay Profiles for (A) TRPL response at 500°C; and (B) Average lifetime and (C) respective energy transfer and distance-dependent values related to GNPs size over ZnO-NR

3.4 Size-Dependent Fluorescence and Quenching Effect

Based on our analysis and results, we believe that the quenching effect in nanoparticles is size-dependent and can be explained using modified Jablonski diagram based on plasmon-coupled energy transfer efficiency and distance-dependent model. The coupled plasmon transitions typically involve between the donor emission and acceptor absorbance in FRET as PC-SET models. Initially, a donor fluorophore absorbs the energy due to the excitation of incident light and transfers the excitation energy to an adjacent ZnO-NR as the acceptor as displayed in Fig. 4A & B. From our experimental data, an ascending trend of the relative lifetime was observed as the fluorophore moved farther away from the particle surface as displayed in Fig.8 (A) where the distance changed with different GNPs sizes reflecting the effects of seeding temperature over ZnO-NR. Distance-dependent ranges do not restrict the FRET model until 100 Å as shown by the dotted line in Fig. 8 (A) [52]. The observed phenomena were supported by the findings of Chhabra et al., which report that the distance dependence of surface energy transfer behavior, i.e., quenching efficiency, is proportional to $1/d^4$.[60] Conversely, it is noted that metallic particles or colloidal particles affect the radiative energy rates of fluorophore dye close to the surface, and surface energy transfer (SET) changes subsequently. It indicates that fluorescence quenching of nearby

molecules is due to small GNP size. Therefore, the emission near the surface of the GNP over ZnO might be quenched by the energy-transfer mechanism where the quenching efficiency affects the size of GNPs Fig.8 (B).

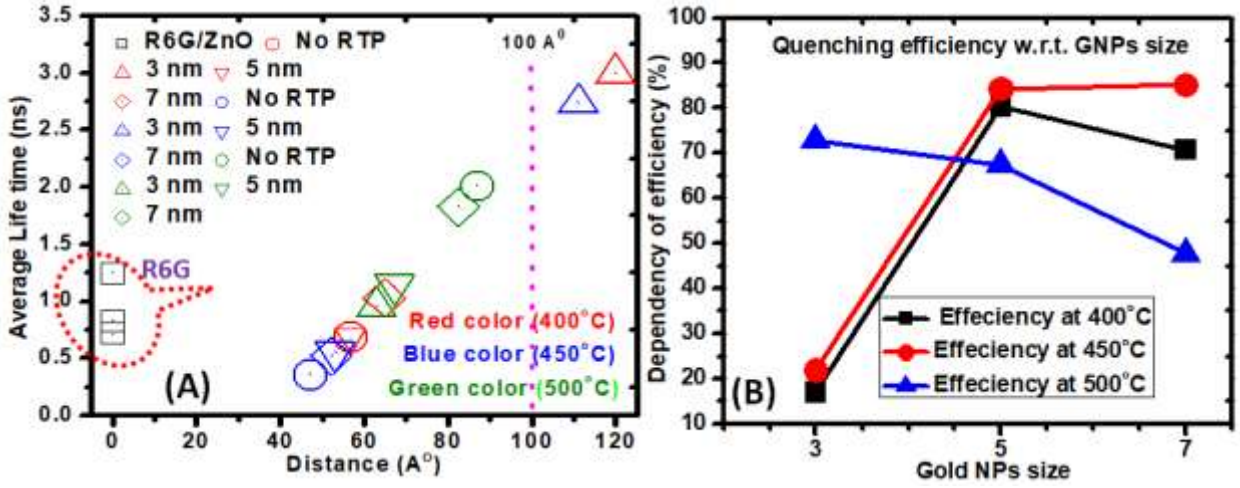

Fig.8 (A) Characteristics of average lifetime vs distance between donor and acceptor; (B) Quenching efficiency variation vs GNPs size.

The stronger quenching efficiencies with smaller sizes of GNPs were in a linear correlation with previously published results on the size-dependent quenching by gold nanoparticles on fluorescence dye. The reason being for this condition can be due to the fact that (1) the bigger GNPs have the lower surface area with a progressive decrease in particle size and can accumulate a large number of probe molecules around the gold particles. As a result, smaller particles become more proficient quenchers of molecular fluorescence than the larger ones. (2) Quantum yield is primarily governed by the non-radiative lifetime and can be approximately equal to radiative lifetime. Researchers also reported similar results highlighting that the rate of non-radiative lifetime increment with particle size is much higher than the radiative lifetime [43]. From the above discussion and reported results, it is evident that strong self-assembly of GNPs over ZnO-NR provides a robust plasmonic surface in which the proposed energy transfer model is highly

potential towards the development of the distance-dependent light-harvesting dual enhanced-fluorescence sensors.

Table 1. Comparison table of previously published plasmon coupled fluorescence emission based on FRET model.

S. No.	**Types of Material/Synthesis/platform model**	**Maximum transfer efficiency (%)**	**Detection of fluorescence emission (As distance ranges) A^0**	**Ref.**
1.	Au NPs/ Solution-based /FRET	55	86.06 to 102.47	[53]
2.	Au@ZnO/ Core-shell colloidal approach/FRET	72.6	67.6 to 88.2	[44]
3.	Au NP-dye conjugate / Chemical synthesis/ SPR / NSET	n/a	68.75 to 118.1	[54]
4.	Au/CdSe (QD)/ Chemical/ Colloidal method/FRET	40.9	95.3 to 110.3	[55]
5.	Acriflavine (Acf)-R6G/ FRET	55.4	74.3 to 61	[7]
6.	GNP–dye/ Solution method / FRET	n/a	n/a	[18]
7.	CDs to MoS2/ Hydrothermal/ Sono chemical method/ FRET	50	n/a	[24]
8.	BODIPY–AuNPs composite/ Solution method/Chemical process/ FRET	n/a	n/a	[25]
9.	**GNPs@ZnO-NR/ Solution-based hydrothermal method/thermal evaporative/ SPR-FRET(Light harvesting mechanism)**	**89.74**	**46.95 - 120**	**Present work**

4. Conclusions

In summary, we have demonstrated a simple, low-cost solution-based defectless ZnO-NR at different seeding temperatures and compared GNPs coated nanostructure over ZnO-NR with other prospective applications together with dual enhanced nature. Additionally, we studied the effect of GNP size and energy transfer efficiency between the dye and Au nanoparticles over ZnO-NR with time-resolved spectroscopy. From the above results, a higher value of distance-dependent was achieved in the proposed structures with the decrease of energy transfer efficiency (ET) correlated to GNPs size over ZnO-NR. Our result affirms that the energy transfer efficiency and distance-dependent do not necessarily increase or decrease together in a plasmonic and non-plasmonic system. However, the larger GNPs with lower surface area and progressive decrease in particle size can accumulate a large number of probe molecules around the gold particles. Therefore, smaller particles become more proficient quenchers of molecular fluorescence than the larger ones. Overall, the proposed development of a light-harvesting PC-SET as dual enhanced sensing model is a novel challenging approach and remarkably envisaged to fill the niche for interdisciplinary works such as in food quality control and drug delivery as a new generation of optical device applications.

Acknowledgments

This research is financially supported by the Ministry of Science and Technology, Taiwan under aproject number of MOST 108-2218-E-182-002 and Chang Gung Memorial Hospital Research Project under a grant number of CMRPD2G0102.

References

[1] Y. Jee, Y. Yu, H.W. Abernathy, S. Lee, T.L. Kalapos, G.A. Hackett, P.R. Ohodnicki, Plasmonic Conducting Metal Oxide-Based Optical Fiber Sensors for Chemical and Intermediate Temperature-Sensing Applications, ACS Appl. Mater. Interfaces. 10 (2018) 42552–42563. https://doi.org/10.1021/acsami.8b11956.

[2] A. Gupta, N. Prabhakar, R. Singh, A. Kaushik, B.D. Malhotra, Sol–gel derived cerium-oxide–silicon-oxide nanocomposite for cypermethrin detection, Thin Solid Films. 519 (2010) 1122–1127. https://doi.org/10.1016/j.tsf.2010.08.055.

[3] A. Purwidyantri, C.H. Hsu, C.M. Yang, B.A. Prabowo, Y.C. Tian, C.S. Lai, Plasmonic nanomaterial structuring for SERS enhancement, RSC Adv. 9 (2019) 4982–4992. https://doi.org/10.1039/c8ra10656h.

[4] A.F.A.A. Melo, A. Hassan, L.J.A. Macedo, I. Osica, L.K. Shrestha, Q. Ji, O.N. Oliveira, J. Henzie, K. Ariga, F.N. Crespilho, Microwires of Au–Ag Nanocages Patterned via Magnetic Nanoadhesives for Investigating Proteins using Surface Enhanced Infrared Absorption Spectroscopy, ACS Appl. Mater. Interfaces. 11 (2019) 18053–18061. https://doi.org/10.1021/acsami.8b21815.

[5] G. Li, C. Cherqui, N.W. Bigelow, G. Duscher, P.J. Straney, J.E. Millstone, D.J. Masiello, J.P. Camden, Spatially Mapping Energy Transfer from Single Plasmonic Particles to Semiconductor Substrates via STEM/EELS, Nano Lett. 15 (2015) 3465–3471. https://doi.org/10.1021/acs.nanolett.5b00802.

[6] J.-F. Li, C.-Y. Li, R.F. Aroca, Plasmon-enhanced fluorescence spectroscopy, Chem. Soc. Rev. 46 (2017) 3962–3979. https://doi.org/10.1039/C7CS00169J.

[7] J. Saha, A.D. Roy, D. Dey, J. Nath, D. Bhattacharjee, S.A. Hussain, Development of arsenic(v) sensor based on Fluorescence Resonance Energy Transfer, Sensors Actuators B Chem. 241 (2017) 1014–1023. https://doi.org/10.1016/j.snb.2016.10.098.

[8] L. Hsu, W. Ding, G.C. Schatz, Plasmon-Coupled Resonance Energy Transfer, J. Phys. Chem. Lett. 8 (2017) 2357–2367. https://doi.org/10.1021/acs.jpclett.7b00526.

[9] S. Kundu, A. Patra, Nanoscale Strategies for Light Harvesting, Chem. Rev. 117 (2017) 712–757. https://doi.org/10.1021/acs.chemrev.6b00036.

[10] B.J. Yun, J.E. Kwon, K. Lee, W.G. Koh, Highly sensitive metal-enhanced fluorescence biosensor prepared on electrospun fibers decorated with silica-coated silver nanoparticles, Sensors Actuators, B Chem. 284 (2019) 140–147. https://doi.org/10.1016/j.snb.2018.12.096.

[11] T. Bora, P. Sathe, K. Laxman, S. Dobretsov, J. Dutta, Defect engineered visible light active ZnO nanorods for photocatalytic treatment of water, Catal. Today. 284 (2017) 11–18. https://doi.org/10.1016/j.cattod.2016.09.014.

[12] B.N.J. Persson, N.D. Lang, Electron-hole-pair quenching of excited states near a metal, Phys. Rev. B. 26 (1982) 5409–5415. https://doi.org/10.1103/PhysRevB.26.5409.

[13] S. Akhavan, M.Z. Akgul, P.L. Hernandez-Martinez, H.V. Demir, Plasmon-Enhanced Energy Transfer in Photosensitive Nanocrystal Device, ACS Nano. 11 (2017) 5430–5439. https://doi.org/10.1021/acsnano.6b08392.

[14] S.K. Cushing, J. Li, J. Bright, B.T. Yost, P. Zheng, A.D. Bristow, N. Wu, Controlling Plasmon-Induced Resonance Energy Transfer and Hot Electron Injection Processes in Metal@TiO 2 Core–Shell Nanoparticles, J. Phys. Chem. C. 119 (2015) 16239–16244. https://doi.org/10.1021/acs.jpcc.5b03955.

[15] K.-S. Kim, S. Il Yoo, B.-H. Sohn, Metal-Coupled Fluorescence Resonance Energy Transfer in Layer-by-Layer Assemblies for Dual Modality Fluorescence Enhancement, Macromol. Chem. Phys. 219 (2018) 1800115. https://doi.org/10.1002/macp.201800115.

[16] A. Zuber, M. Purdey, E. Schartner, C. Forbes, B. Van Der Hoek, D. Giles, A. Abell, T. Monro, H. Ebendorff-Heidepriem, Detection of gold nanoparticles with different sizes using absorption and fluorescence based method, Sensors Actuators, B Chem. 227 (2016) 117–127. https://doi.org/10.1016/j.snb.2015.12.044.

[17] M.M. Elsutohy, A. Selo, V.M. Chauhan, S.J.B. Tendler, J.W. Aylott, Enhanced distance-dependent fluorescence quenching using size tuneable core shell silica nanoparticles, RSC Adv. 8 (2018) 35840–35848. https://doi.org/10.1039/C8RA05929B.

[18] S. Verma, B. Tirumala Rao, A.K. Srivastava, H.S. Patel, S. Satapathy, M.P. Joshi, V.K. Sahu, L.M. Kukreja, Studies on interdependent optical properties of Rhodamine 6G dye and gold nanoparticles at different dilutions of aqueous solutions, J. Lumin. 155 (2014) 156–164.

[19] C.K. Kim, R.R. Kalluru, J.P. Singh, A. Fortner, J. Griffin, G.K. Darbha, P.C. Ray, Gold-nanoparticle-based miniaturized laser-induced fluorescence probe for specific DNA hybridization detection: studies on size-dependent optical properties, Nanotechnology. 17 (2006) 3085–3093. https://doi.org/10.1088/0957-4484/17/13/001.

[20] C. Duan, H. Cui, Z. Zhang, B. Liu, J. Guo, W. Wang, Size-Dependent Inhibition and Enhancement by Gold Nanoparticles of Luminol−Ferricyanide Chemiluminescence, J. Phys. Chem. C. 111 (2007) 4561–4566. https://doi.org/10.1021/jp068801x.

[21] P. Reineck, D. Gómez, S.H. Ng, M. Karg, T. Bell, P. Mulvaney, U. Bach, Distance and Wavelength Dependent Quenching of Molecular Fluorescence by Au@SiO 2 Core–Shell

Nanoparticles, ACS Nano. 7 (2013) 6636–6648. https://doi.org/10.1021/nn401775e.

[22] C. Xue, Y. Xue, L. Dai, A. Urbas, Q. Li, Size- and Shape-Dependent Fluorescence Quenching of Gold Nanoparticles on Perylene Dye, Adv. Opt. Mater. 1 (2013) 581–587. https://doi.org/10.1002/adom.201300175.

[23] V.K. Sonu, S. Mitra, Quenching of Luminol Fluorescence at Nano-Bio Interface: Towards the Development of an Efficient Energy Transfer System, J. Fluoresc. 29 (2019) 165–176. https://doi.org/10.1007/s10895-018-2324-2.

[24] S. Gogoi, R. Khan, Fluorescence immunosensor for cardiac troponin T based on Förster resonance energy transfer (FRET) between carbon dot and MoS 2 nano-couple, Phys. Chem. Chem. Phys. 20 (2018) 16501–16509. https://doi.org/10.1039/C8CP02433B.

[25] J. Xu, H. Yu, Y. Hu, M. Chen, S. Shao, A gold nanoparticle-based fluorescence sensor for high sensitive and selective detection of thiols in living cells, Biosens. Bioelectron. 75 (2016) 1–7. https://doi.org/10.1016/j.bios.2015.08.007.

[26] C.M. Chang, M.H. Hon, I.C. Leu, Influence of Size and Density of Au Nanoparticles on ZnO Nanorod Arrays for Sensing Reducing Gases, J. Electrochem. Soc. 160 (2013) B170–B176. https://doi.org/10.1149/2.076309jes.

[27] A.K. Gupta, C. Hsu, C. Chen, A. Purwidyantri, B.A. Prabowo, J.-L. Wang, Y.-C. Tian, C. Lai, Au-spotted zinc oxide nano-hexagonrods structure for plasmon-photoluminescence sensor, Sensors Actuators B Chem. 290 (2019) 100–109. https://doi.org/10.1016/j.snb.2019.03.020.

[28] S. Boubenia, A.S. Dahiya, G. Poulin-Vittrant, F. Morini, K. Nadaud, D. Alquier, A facile hydrothermal approach for the density tunable growth of ZnO nanowires and their electrical characterizations, Sci. Rep. 7 (2017) 15187. https://doi.org/10.1038/s41598-017-

15447-w.

[29] A. Purwidyantri, I.I. El-Mekki, C.C.-S.C.-S. Lai, Tunable Plasmonic SERS “Hotspots” on Au-Film Over Nanosphere by Rapid Thermal Annealing, IEEE Trans. Nanotechnol. 16 (2017) 551–559. http://ieeexplore.ieee.org/document/7803554/.

[30] J. Kegel, V.Z. Zubialevich, M. Schmidt, I.M. Povey, M.E. Pemble, Effect of Surface and Defect Chemistry on the Photocatalytic Properties of Intentionally Defect-Rich ZnO Nanorod Arrays, ACS Appl. Mater. Interfaces. 10 (2018) 17994–18004. https://doi.org/10.1021/acsami.8b05130.

[31] T. Bora, M.T.Z. Myint, S.H. Al-Harthi, J. Dutta, Role of surface defects on visible light enabled plasmonic photocatalysis in Au–ZnO nanocatalysts, RSC Adv. 5 (2015) 96670–96680. https://doi.org/10.1039/C5RA16569E.

[32] J.D. Hwang, F.H. Wang, C.Y. Kung, M.J. Lai, M.C. Chan, Annealing effects of Au nanoparticles on the surface-plasmon enhanced p-Si/n-ZnO nanorods heterojunction photodetectors, J. Appl. Phys. 115 (2014) 173110. https://doi.org/10.1063/1.4875657.

[33] X. Zhang, J. Qin, Y. Xue, P. Yu, B. Zhang, L. Wang, R. Liu, Effect of aspect ratio and surface defects on the photocatalytic activity of ZnO nanorods, Sci. Rep. 4 (2014) 4596. https://doi.org/10.1038/srep04596.

[34] S. Lu, J. Qi, S. Liu, Z. Zhang, Z. Wang, P. Lin, Q. Liao, Q. Liang, Y. Zhang, Piezotronic Interface Engineering on ZnO/Au-Based Schottky Junction for Enhanced Photoresponse of a Flexible Self-Powered UV Detector, ACS Appl. Mater. Interfaces. 6 (2014) 14116–14122. https://doi.org/10.1021/am503442c.

[35] J.-D. Chen, J. Xiang, S. Jiang, Q.-F. Dai, S.-L. Tie, S. Lan, Radiation of the high-order plasmonic modes of large gold nanospheres excited by surface plasmon polaritons,

Nanoscale. 10 (2018) 9153–9163. https://doi.org/10.1039/C8NR02099J.

[36] B. Kafle, P. Gieri, H. Kookhaee, T.E. Tesema, S. Haq, A. Manjavacas, T.G. Habteyes, Robust Charge Transfer Plasmons in Metallic Particle–Film Systems, ACS Photonics. 5 (2018) 4022–4029. https://doi.org/10.1021/acsphotonics.8b00554.

[37] D. Lee, J. Lee, J. Song, M. Jen, Y. Pang, Homogeneous silver colloidal substrates optimal for metal-enhanced fluorescence, Phys. Chem. Chem. Phys. 21 (2019) 11599–11607. https://doi.org/10.1039/C9CP00585D.

[38] H. Mishra, B.L. Mali, J. Karolin, A.I. Dragan, C.D. Geddes, Experimental and theoretical study of the distance dependence of metal-enhanced fluorescence, phosphorescence and delayed fluorescence in a single system, Phys. Chem. Chem. Phys. 15 (2013) 19538. https://doi.org/10.1039/c3cp50633a.

[39] S. Pawar, A. Bhattacharya, A. Nag, Metal-Enhanced Fluorescence Study in Aqueous Medium by Coupling Gold Nanoparticles and Fluorophores Using a Bilayer Vesicle Platform, ACS Omega. 4 (2019) 5983–5990. https://doi.org/10.1021/acsomega.9b00036.

[40] N. Sui, L. Wang, T. Yan, F. Liu, J. Sui, Y. Jiang, J. Wan, M. Liu, W.W. Yu, Selective and sensitive biosensors based on metal-enhanced fluorescence, Sensors Actuators, B Chem. 202 (2014) 1148–1153. https://doi.org/10.1016/j.snb.2014.09.075.

[41] M. Abd-Ellah, N. Moghimi, L. Zhang, J.P. Thomas, D. McGillivray, S. Srivastava, K.T. Leung, Plasmonic gold nanoparticles for ZnO-nanotube photoanodes in dye-sensitized solar cell application, Nanoscale. 8 (2016) 1658–1664. https://doi.org/10.1039/C5NR08029K.

[42] C. Hauswald, T. Flissikowski, T. Gotschke, R. Calarco, L. Geelhaar, H.T. Grahn, O. Brandt, Coupling of exciton states as the origin of their biexponential decay dynamics in

GaN nanowires, Phys. Rev. B. 88 (2013) 075312. https://doi.org/10.1103/PhysRevB.88.075312.

[43] J. Bohlen, Á. Cuartero-González, E. Pibiri, D. Ruhlandt, A.I. Fernández-Domínguez, P. Tinnefeld, G.P. Acuna, Plasmon-assisted Förster resonance energy transfer at the single-molecule level in the moderate quenching regime, Nanoscale. 11 (2019) 7674–7681. https://doi.org/10.1039/C9NR01204D.

[44] K.K. Haldar, T. Sen, A. Patra, Au@ZnO Core−Shell Nanoparticles Are Efficient Energy Acceptors with Organic Dye Donors, J. Phys. Chem. C. 112 (2008) 11650–11656. https://doi.org/10.1021/jp8031308.

[45] R.R. Chance, A. Prock, R. Silbey, Molecular Fluorescence and Energy Transfer Near Interfaces, in: Wiley Sons, 1978: pp. 1–65. http://doi.wiley.com/10.1002/9780470142561.ch1.

[46] T.L. Jennings, M.P. Singh, G.F. Strouse, Fluorescent Lifetime Quenching near d = 1.5 nm Gold Nanoparticles: Probing NSET Validity, J. Am. Chem. Soc. 128 (2006) 5462–5467. https://doi.org/10.1021/ja0583665.

[47] J. Griffin, A.K. Singh, D. Senapati, P. Rhodes, K. Mitchell, B. Robinson, E. Yu, P.C. Ray, Size- and Distance-Dependent Nanoparticle Surface-Energy Transfer (NSET) Method for Selective Sensing of Hepatitis C Virus RNA, Chem. - A Eur. J. 15 (2009) 342–351. https://doi.org/10.1002/chem.200801812.

[48] R. Chhabra, J. Sharma, H. Wang, S. Zou, S. Lin, H. Yan, S. Lindsay, Y. Liu, Distance-dependent interactions between gold nanoparticles and fluorescent molecules with DNA as tunable spacers, Nanotechnology. 20 (2009) 485201. https://doi.org/10.1088/0957-4484/20/48/485201.

[49] A. Safavi, G. Absalan, F. Bamdad, Effect of gold nanoparticle as a novel nanocatalyst on luminol–hydrazine chemiluminescence system and its analytical application, Anal. Chim. Acta. 610 (2008) 243–248. https://doi.org/10.1016/j.aca.2008.01.053.

[50] J.R. Lakowicz, B.R. Masters, Principles of Fluorescence Spectroscopy, Third Edition, J. Biomed. Opt. 13 (2008) 029901. http://biomedicaloptics.spiedigitallibrary.org/article.aspx?doi=10.1117/1.2904580.

[51] J.I. Gersten, A. Nitzan, Photophysics and photochemistry near surfaces and small particles, Surf. Sci. 158 (1985) 165–189. https://doi.org/10.1016/0039-6028(85)90293-6.

[52] P.C. Ray, Z. Fan, R.A. Crouch, S.S. Sinha, A. Pramanik, Nanoscopic optical rulers beyond the FRET distance limit: fundamentals and applications, Chem. Soc. Rev. 43 (2014) 6370–6404. https://doi.org/10.1039/C3CS60476D.

[53] T. Sen, S. Sadhu, A. Patra, Surface energy transfer from rhodamine 6G to gold nanoparticles: A spectroscopic ruler, Appl. Phys. Lett. 91 (2007) 043104. https://doi.org/10.1063/1.2762283.

[54] M.P. Singh, G.F. Strouse, Involvement of the LSPR Spectral Overlap for Energy Transfer between a Dye and Au Nanoparticle, J. Am. Chem. Soc. 132 (2010) 9383–9391. https://doi.org/10.1021/ja1022128.

[55] K.K. Haldar, T. Sen, A. Patra, Metal Conjugated Semiconductor Hybrid Nanoparticle-Based Fluorescence Resonance Energy Transfer, J. Phys. Chem. C. 114 (2010) 4869–4874. https://doi.org/10.1021/jp911348n.

Graphical Abstract